Thermal Expansion of Confined Water

Shuangyan Xu,[†,§] George W. Scherer,[*,†] T. S. Mahadevan,[‡] and Stephen H. Garofalini[‡]

[†]*Civil & Environmental Engineering/PRISM, Eng. Quad. E-319, Princeton University, Princeton, New Jersey 08544 and [‡]Interfacial Molecular Science Laboratory, Department of Materials Science & Engineering, Rutgers University, Piscataway, New Jersey 08855. [§] Present address: Applied Materials Xi'an, 28 Xinxi Road, Xi'an Hi-Tech Industrial Development Zone, Xi'an, Shaanxi, PRC 710119.*

Dilatometric measurement of the thermal expansion of water in porous silica shows that the expansion coefficient increases systematically as the pore size decreases below about 15 nm. This behavior is quantitatively reproduced by molecular dynamics (MD) simulations based on a new dissociative potential. According to MD, the structure of the water is modified within ~6 Å of the pore wall, so that it resembles bulk water at a higher pressure. On the basis of this observation, it is possible to account for the measured expansion, as the thermal expansion coefficient of bulk water increases with temperature over the range considered in this study.

1. Introduction

The structural, dynamical, and physical properties of liquids in confined spaces have been the subject of many computational and experimental studies [e.g., ref 1]. In the present work, we examine the anomalously high thermal expansion coefficient of water confined in nanometric pores of silica xerogels and porous glass. Our attention was first drawn to this problem during a study of the thermal response of cement paste, which indirectly indicated that the thermal expansion coefficient of the fluid in cement paste is significantly larger than that of bulk water (or aqueous solution); direct dilatometric measurements confirmed that the thermal expansion coefficient in the paste was 30−60% higher than in bulk liquid.[2] This phenomenon is of practical importance because thermal expansion stresses from sudden heating (as in a fire) can produce cracks that raise the permeability and reduce the strength of concrete, even leading to structural failure. Motivated by the observation made on cement pastes, and in order to have a better understanding of the physical properties of liquids in small pores, we have measured the thermal expansion and viscosity of water in a series of porous glasses with controlled pore size in this work. This is an extension of an experimental study reported earlier.[3] To interpret the experiments, we have preformed simulations using molecular dynamics (MD) with a novel dissociative potential.[4]

Derjaguin et al.[5,6] were apparently the first to investigate the thermal expansion of water in small pores. Using a

dilatometric method, they measured the expansion of water in the pores of silica xerogels and observed that the expansion is anomalously high compared to that of bulk water and the water density does not reach its maximum at 4 °C. They inferred that water in small pores exhibits an increased density. However, Takei et al.[7] and Etzler et al.[8] found that the density of water in silica pores is lower than that of the bulk water, which is contradictory to the observation by Derjaguin et al. Measurements of the expansion of water in the pores of Vycor glasses with pore diameters of 5 and 7.4 nm showed elevated expansion but did not permit absolute density values to be determined.[3] In the present work, the range of pore sizes is extended to 3−13 nm. The materials and methods employed are described in sections 2 and 3.

Molecular dynamics (MD) studies of water in Vycor glass by Ricci and co-workers[9,10] suggested that water near the pore wall is hydrogen-bonded, but the network is strongly distorted relative to bulk water. They concluded that the structure of the confined water in the inner layer, close to the center of the pore, is similar to the structure of bulk water at a temperature 30 °C higher than that of the simulation. As we shall see, that is the opposite of the conclusion of our work. MD results obtained by Spohr et al.[11] indicated that two layers of water molecules are strongly affected by the silica surface; the mobility of water molecules directly attached to the pore surface is reduced by more than 1 order of magnitude, while the mobility of molecules in the inner layer is comparable to that of the bulk water. Differential scanning calorimetry (DSC) and X-ray diffraction studies performed by Fousri et al.[12] suggested the presence of a distorted tetrahedral hydrogen-bonded network of water in silica gel, and they concluded that the distortion is a result of a competition between the confinement effect and water−silica interaction.

---

*To whom correspondence should be addressed. E-mail: scherer @princeton.edu.

(1) *Dynamics of Small Confining Systems*; Mater. Res. Soc. Symp. Proc. Vol. *790*; Fourkas, J. T., Levitz, P., Urbakh, M., Wahl, K. J., Eds.; Materials Research Society: Warrendale, **2004**.
(2) Valenza, J. J.; Scherer, G. W. *Cem. Concr. Res.* **2005**, *35*, 57−66.
(3) Xu, S.; Simmons, G. C.; Scherer, G. W. In *Dynamics of Small Confining Systems*; Mater. Res. Soc. Symp. Proc. Vol. *790*; Fourkas, J. T., Levitz, P., Urbakh, M., Wahl, K. J., Eds.; Materials Research Society: Warrendale, **2004**; pp 85−91.
(4) Mahadevan, T. S.; Garofalini, S. H. *J. Phys. Chem. B* **2007**, *111*, 8919−8927.
(5) Karasev, V. V.; Derjaguin, B. V.; Khromova, E. N. In *Collection Researches in Surface Forces*; Consultants Bureau: New York, **1971**; Vol. *3*, pp 25−28.
(6) Derjaguin, B. V.; Karasev, V. V.; Khromova, E. N. *J. Colloid Interface Sci.* **1986**, *109*, 586−587.

---

(7) Takei, T.; Mukasa, K.; Fuji, M.; Watanabe, T.; Chikazawa, M.; Kanazawa, T. *Colloid Polym. Sci.* **2000**, *278*, 475.
(8) Etzler, F. M.; Fagundus, D. M. *J. Colloid Interface Sci.* **1987**, *115*, 513.
(9) Gallo, P.; Ricci, M. A.; Rovere, M. *J. Chem. Phys.* **2002**, *116*, 342−346.
(10) Soper, A. K.; Bruni, R.; Ricci, M. A. *J. Chem. Phys.* **1998**, *109*, 1486−1494.
(11) Spohr, E.; Hartning, C.; Gallo, P.; Rovere, M. *J. Mol. Liq.* **1999**, *80*, 165.
(12) Fousri, A.; Sorbez-Sridi, R.; Oumezzine, M. *Eur. Phys. J. AP* **2003**, *22*, 21.

Since the anomalous behavior of interest is related to the interaction of water with the pore walls, and given that water reacts with silica to create silanol groups,[13] we think it is essential for MD investigations of confined water to use a dissociative potential. The version used in this paper has been shown to reproduce the equation of state over a broad range of temperature and pressure and to yield the correct structure and properties of bulk water.[4] Application of this dissociative water potential to simulations of silica glass exposed to water showed the correct formation of silanols (SiOH) in a concentration consistent with experiment and the formation of hydronium ions consistent with ab initio calculations and interpretations of experiment.[14] The potentials and the method used in the simulations are discussed in section 4, and the results are used to interpret the experiments in section 5.

2. Experimental Procedure

The porous hosts included two samples of Vycor glass (kindly provided by Corning, Inc.) with pore diameters of about 5 and 7.4 nm. To remove organic impurities from the pores, the rods were boiled in a 30% solution of hydrogen peroxide for several hours until the rods turned clear, then rinsed in deionized water, and stored in ethanol. Before measurements, the samples were exchanged into water by submerging them in a volume much larger (at least 15 times higher) than the volume of rods for at least 12 h. To obtain a broader range of pore sizes, we also used a silica xerogel made from tetramethoxysilane[15] that had been made for an unrelated study years earlier and had dried very slowly to yield uncracked cylinders with diameters of a few millimeters. An aerogel was made by exchanging a silica gel into alcohol, and then into CO_2, followed by supercritical drying; it was then sintered in a helium atmosphere at 1050 °C for 9 h. Pore size distributions were calculated by the BJH method[16] from a nitrogen desorption curve measured using a Micromeritics ASAP 2010.

Following Derjaguin et al.,[6] the coefficient of thermal expansion (CTE) of water confined in glass samples was measured using a dilatometer. The basic principle of this method is to measure the amount of liquid flowing out of the porous silica glasses as the temperature increases in a test. The experimental apparatus illustrated in Figure 1 consists of a water bath (Isotemp 3006), two identical glass bulbs, a linear variable differential transformer (LVDT, MacroSensors), an optical probe (MTI 1000, Fotonic Sensor) for position measurements, a stepper motor that controls the vertical movement of the optical probe, and a computer that collects data. Before testing, the saturated sample and a carefully measured mass of additional water were put into the sample bulb. The sample tube was then evacuated in a closed container for several minutes to remove any air bubbles trapped in the liquid. A layer of oil containing Oil Red (Acros) was placed on top of the water in the neck of the bulb to reflect the light emitted from the optical probe and to hinder the water in the bulb from evaporating throughout a test. An identical glass bulb filled with the same amount of sample and bulk liquid was also prepared. Both bulbs were then held in the water bath as shown in Figure 1. Three thermocouples were utilized, two being inserted in the reference bulb to measure the temperature in the bulb and the third one being used to check the temperature of the water bath during the test. The optical probe was placed above the oil surface in the sample bulb and turned on before testing. It was calibrated before each measurement using the LVDT (range 0−10 mm), which was
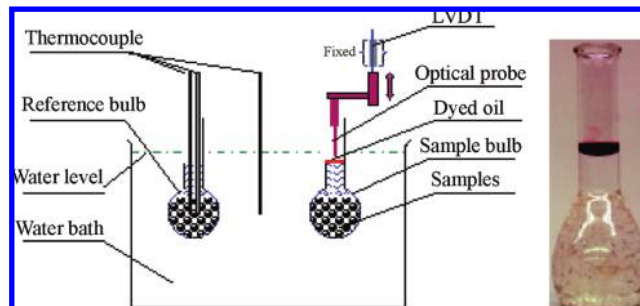

Figure 1. Schematic of the experimental apparatus for thermal expansion measurements. The right picture shows the actual sample bulb with porous glass samples inside.

placed on the top of a translation stage (Oriel) connected to the optical probe. The stage moved the optical probe away from the oil surface, and the displacement measured by the LVDT was used to calibrate the probe. The probe was fixed at a position above the oil surface at each temperature interval between 10 and 40 °C. As the bath temperature increased, the liquid in the bulb expanded, and the decrease in distance between the oil surface and the probe tip was measured.

The specific volume of the confined liquid v_{cf} at each test temperature was needed to determine the thermal expansion of the confined water. It was calculated using the following equation:

$$\rho_{cf} = \frac{1}{v_{cf}} = \frac{m_i - \rho_b V_{out}}{V_p(1 + \alpha_{solid}(T - T_i))} \quad (1)$$

where ρ_{cf} is the density of confined fluid in the pores; V_p is the pore volume of the porous glass, which was determined by nitrogen adsorption; α_{solid} is the volumetric CTE of the solid phase of the test sample, which was measured separately; m_i is the initial mass of confined water in the pores; ρ_b is the density of bulk water; V_{out} is the volume of the confined water flowing out of the pores as the test temperature is increased to T from the initial test temperature T_i. V_{out} is the total volume change measured in the test after subtracting the volume changes caused by the expansions of the dyed oil, the sample bulb, and the original bulk liquid and the glass in the sample bulb as the test temperature rises.

After the specific volume of the confined liquid v_{cf} at each test temperature was determined, the thermal expansion of the confined liquid at the test temperature was obtained by plotting the natural logarithm of v_{cf} as a function of the test temperature and calculating the slope of the curve of $\ln(v_{cf})$ vs T, which was fitted using a second-order polynomial curve:

$$\alpha = \frac{1}{v_{cf}}\frac{\Delta v_{cf}}{\Delta T} = \frac{d \ln(v_{cf})}{dT} \quad (2)$$

Before making the measurements on the confined liquid, the CTE of bulk water was measured using exactly the same method, except that the porous glass was replaced by solid glass beads to reduce the volume of liquid to match that in the measurements using porous glass. Typical results for expansion measurements on the bulk liquid, reported in ref 3, agreed with the handbook values with errors < 5%.

The dilatometric experiments were repeated with 1 M solutions of NaCl and $CaCl_2$ to investigate the influence of dissolved ions on the expansion.

3. Results

The pore size distributions for the samples are shown in Figure 2. None is strictly unimodal, but each is narrow and

(13) Iler, R. K. *The Chemistry of Silica*; Wiley: New York, **1979**.
(14) Mahadevan, T. S.; Garofalini, S. H. *J. Phys. Chem. C* **2008**, *112*, 1507−1515.
(15) Brinker, C. J.; Scherer, G. W. *Sol-Gel Science*; Academic Press: New York, **1990**; Chapter 3.
(16) Lowell, S.; Shields, J. E. *Powder Surface Area and Porosity*; Chapman and Hall: New York, **1984**.
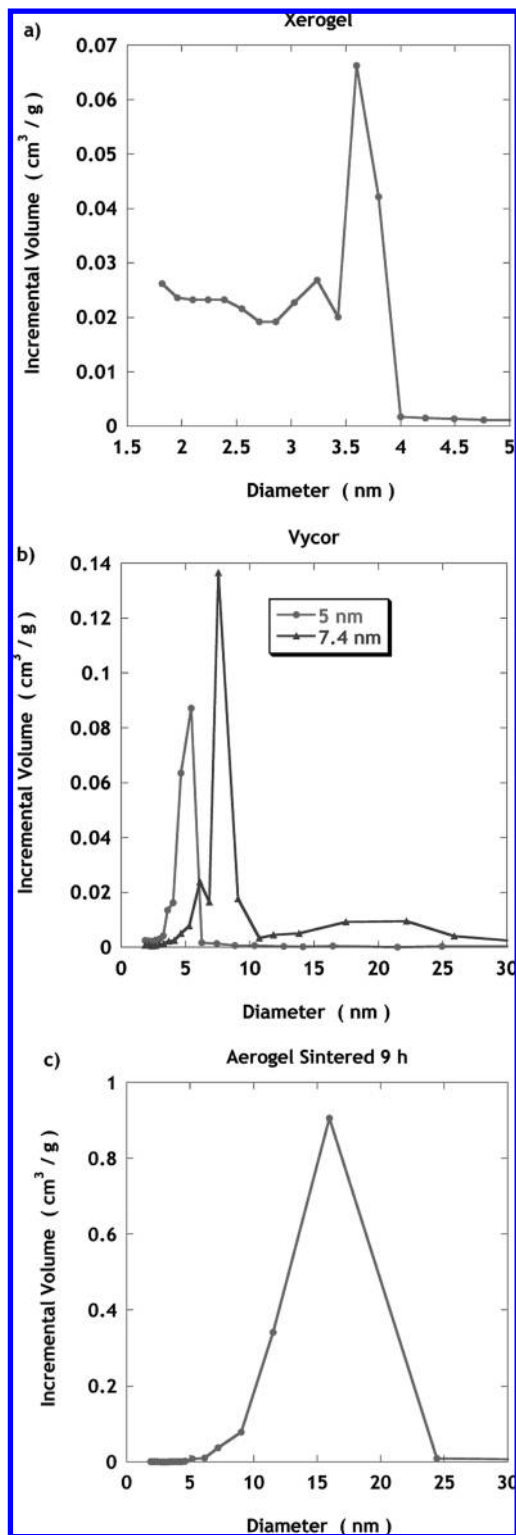
Figure 2. Pore size distributions measured by nitrogen desorption for (a) silica xerogel, (b) Vycor porous glass, and (c) sintered aerogel.

Table 1. Pore Characterization

sample ID	surface area[a] (m^2/g)	pore volume[b] (cm^3/g)	pore diameter[c] (nm)	porosity[d]
Vycor 5 nm	179	0.204	4.55	0.305
Vycor 7 nm	137	0.253	7.40	0.352
Xerogel 3 nm	628	0.370	2.85	0.425
Aerogel 13 nm	347	1.42	13.4	0.758

[a] BET surface area. [b] Nitrogen adsorption (cumulative). [c] From nitrogen pore volume, V, and area, A: diameter = $4V/A$. [d] Calculated assuming skeletal density of 2.0 g/cm^3 for xerogel, 2.15 g/cm^3 for Vycor, and 2.2 g/cm^3 for sintered aerogel.
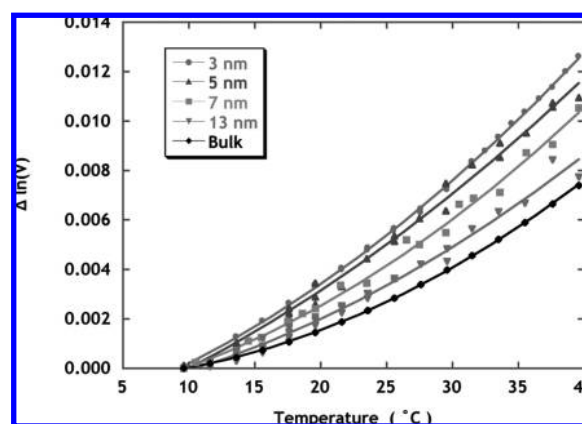

Figure 3. Volumetric expansion of pure water in bulk or confined in porous glass with the indicated average pore diameter, where $\Delta \ln (V) = \ln V(T) - \ln V(9.6\,°C)$. The slope of the curve is the volumetric thermal expansion coefficient.
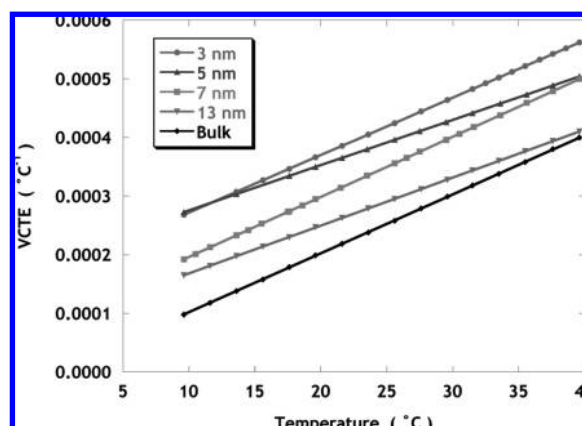

Figure 4. Volumetric thermal expansion coefficient of confined and bulk water, obtained from the slopes of the curves shown in Figure 3.

distinct from the others. The surface area, pore volume, mean pore size, and porosity are listed in Table 1.

The volume of the pore water as a function of temperature is shown in Figure 3. Data were collected from about 10 to 40 °C, and the results are arbitrarily shifted relative to the value at 9.6 °C; that is, $\Delta \ln V = \ln V(T) - \ln V(9.6\,°C)$. The CTE of the pore liquid is found from the slopes of these curves; the results are shown in Figure 4. The ratio of the CTE of the confined liquid to that of bulk water at the same temperature is shown in Figure 5. The ratio rises rapidly at low temperature because the CTE of bulk water goes to zero at about 4 °C, but that of the confined water remains positive at lower temperatures.[5] As shown in Figure 6, the rise is smaller for the salt solutions because their temperature of maximum density is lower. What is most significant is that the enhancement of α_L caused by confinement of the 1 M NaCl solution is nearly identical to that of bulk water above ∼20 °C, suggesting that those ions have relatively little effect on the structure of water in the pores. In contrast, the expansion of the 1 M solution of calcium chloride is raised significantly more by confinement than pure water. Since the anions are the same in
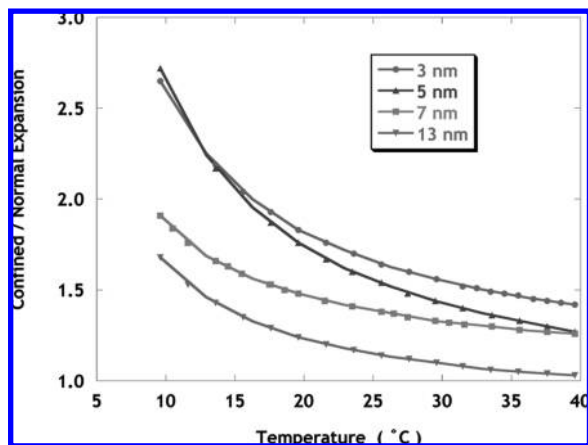
Figure 5. Ratio of the thermal expansion coefficient of confined water to that of bulk water at the same temperature.

these two solutions, we conclude that the divalent Ca^{2+} ion influences the water structure significantly in the small pores.

4. Molecular Dynamics Simulations

While many water potentials exist,[17−35] most are nondissociating, being either rigid or at most flexible. In general, the properties of water can be expressed fairly accurately over a narrow range of temperatures and pressures with these potentials. One major problem has been the failure of these potentials to reproduce the density vs temperature curve over the liquid state range from 273 to 373 K.[29] Even in cases where the temperature of maximum density is reproduced, the potentials often fail at reproducing the rest of the liquid state density−temperature curve.[34] Since our major interest is in the behavior of water interacting with oxide pore surfaces and the atomistic evaluation of the anomalous expansion of confined water and solutions, the exact reproduction of the bulk liquid expansion curve becomes paramount. We also want to include the dissociation of water onto the silica surface in order to compare to the experimental data, similar to earlier simulations of water on silica,[36] but with a more accurate water potential. Other dissociative water potentials exist but are similarly not sufficiently accurate with respect to the liquid
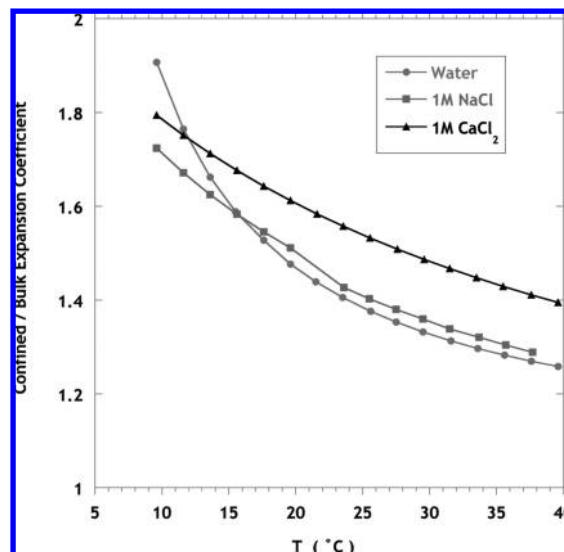
(17) Rahman, A.; Stillinger, F. H. *J. Chem. Phys.* **1971**, *55*, 3336–3359.
(18) Rahman, A.; Stillinger, F.; Lemberg, H. *J. Chem. Phys.* **1975**, *63*, 5223–5230.
(19) Stillinger, F.; Rahman, A. *J. Chem. Phys.* **1978**, *68*, 666–670.
(20) Jorgensen, W. L. *J. Am. Chem. Soc.* **1981**, *103*, 335–340.
(21) Jorgensen, W. L.; Chandrasekhar, J.; Madura, J. D.; Impey, R. W.; Klein, M. L. *J. Chem. Phys.* **1983**, *83*, 926–935.
(22) Weber, T.; Stillinger, F. *J. Phys. Chem.* **1982**, *86*, 1314–1318.
(23) Jorgensen, W. *J. Chem. Phys.* **1982**, *77*, 4156–4163.
(24) Zhu, S.-B.; Singh, S.; Robinson, G. W. *J. Chem. Phys.* **1991**, *95*, 2791–2799.
(25) Sprik, M. *J. Chem. Phys.* **1991**, *95*, 6762–6769.
(26) Halley, J. W.; Rustad, J. R.; Rahman, A. *J. Chem. Phys.* **1993**, *98*, 4110–4119.
(27) Rick, S. W.; Stuart, S. J.; Berne, B. J. *J. Chem. Phys.* **1994**, *101*, 6141–6156.
(28) Dang, L.; Chang, T.-M. *J. Chem. Phys.* **1997**, *106*, 8149–8159.
(29) Mahoney, M. W.; Jorgensen, W. L. *J. Chem. Phys.* **2000**, *112*, 8910–8922.
(30) Stern, H. A.; Rittner, F.; Berne, B. J.; Friesner, R. A. *J. Chem. Phys.* **2001**, *115*, 2237–2251.
(31) Guillot, B.; Guissani, Y. *J. Chem. Phys.* **2001**, *114*, 6720–6733.
(32) Izvekov, S.; Parrinello, M.; Burnham, C. J.; Voth, G. A. *J. Chem. Phys.* **2004**, *120*, 10896–10913.
(33) Ren, P.; Ponder, J. W. *J. Phys. Chem. B* **2003**, *107*, 5933–5947.
(34) Ren, P.; Ponder, J. W. *J. Phys. Chem. B* **2004**, *108*, 13427–13437.
(35) Paricaud, P.; Predota, M.; Chialvo, A. A.; Cummings, P. T. *J. Chem. Phys.* **2005**, *122*, 244511.
(36) Feuston, B. P.; Garofalini, S. H. *J. Appl. Phys.* **1990**, *68*, 4830–4836.

Figure 6. Ratio of the volumetric thermal expansion coefficients for confined and bulk liquids, where the confined solutions are in 7 nm diameter pores of Vycor glass.

equation of state. To obtain a more appropriate water potential, we modified the rigid water potential developed by Guillot and Guissani,[31] so that it more accurately reproduced the features of bulk water but also allowed for dissociation. This newly developed water potential[4] uses a multibody potential, with both pair and three-body terms, and the Wolf summation method for the long-range Coulomb interactions.[37] Details regarding the parameters are given in ref 4.

A major feature of this potential is its ability to reproduce the experimental density−temperature curve of liquid water between 273 and 373 K at 1 atm[38] (plus a datum at 263 K[39]) using only a change in the short-range repulsive term in the O−H interaction as a function of temperature and pressure. The details of this approach were discussed in ref 4. An important result of this methodology is that the simulations also reproduce other room temperature properties of water, such as structure, cohesive energy, diffusion constant, and vibrational spectra as well as the liquid−vapor coexistence curve. The pair distribution functions (PDF) of the OO, OH, and HH pairs at 298 K are in excellent agreement with experiment. This potential is the basis of our subsequent simulations of confined liquids.

The simulations of confined water required formation of the silica glass followed by inclusion of the water. The silica glass was prepared using a simulated melt−quench process using periodic boundaries. The silica included 11 664 Si and O atoms that went through a melt at 6000 K, followed by cooling to 300 K via intermediate temperatures in a manner similar to that previously published.[14] The system size at 300 K is approximately 64 Å × 64 Å × 43 Å in *x*, *y*, and *z*, respectively. Water molecules were added on top of the silica glass so that a 30 Å layer and a 70 Å layer of water could be studied. Periodic boundaries meant that the water slab was confined between the silica glass on top and bottom (in *z*) but "infinite" in the *x* and *y* directions. Two different systems of water confined in

(37) Wolf, D.; Keblinski, P.; Phillpot, S. R.; Eggebrecht, J. *J. Chem. Phys.* **1999**, *110*, 8254−8282.
(38) Wagner, W.; Cooper, J. R.; Dittmann, A.; Kijima, J.; Kretzchmar, H.-J.; Kruse, A.; Mares, R.; Oguchi, K.; Sato, H.; Stocker, I.; Sifner, O.; Takaishi, Y.; Tanishita, I.; Trubenbach, J.; Willkommen, T. *ASME J. Eng. Gas Turbines Power* **2000**, *122*, 150−182.
(39) Hare, D. E.; Sorensen, C. M. *J. Chem. Phys.* **1986**, *84*, 5085.

the same silica were simulated for the 30 Å system. In one, the water/glass system was run at 283, 293, 298, 313, 323, and 333 K, while the second set was run at 283, 293, 298, 310, 313, and 323 K. In all cases, the runs were for 1 000 000 time steps at each temperature under modified NPT (constant number, pressure, temperature) conditions. The modification was that the x and y dimensions were unchanged while the z dimension responded to a constant pressure of 1 atm in that direction. The time step of 0.1 fs was used in all simulations with water molecules present because of the H ions. The z dimension of each system reached the equilibrium value at each specific temperature within ~200 000 time steps. Dimensional data were averaged over the last 40% of each run. The $V(T)$ data for bulk silica alone were also simulated at the same temperatures and 1 atm pressure in z and subtracted from the $V(T)$ data of the water/silica system so that the $V(T)$ data of the water could be determined. Most results presented here will relate to the 30 Å film, since relevant results are similar in the 70 Å film as well. Some of the results on the simulation of confined water have recently been reported.[40]

5. Results and Discussion

Figure 7 shows the expansion results of the MD simulations for the 3 and 7 nm films compared to the experimental data for water confined in 3 and 7 nm pores as well as the results for bulk water expansion (which is similar for both the simulations and the experiment).[4] The simulations show the same trends of increasing expansion with decreasing pore size seen experimentally. Most importantly, parameters in the potential were not changed in the simulations of the confined water from those developed from the bulk water simulations.

The density of atoms as a function of distance perpendicular to the interfaces for the 30 Å film at 298 K and 1 atm is shown in Figure 8 and has been previously shown.[40] Unlike other simulations of nanoconfined water using nondissociative water potentials that showed large density increases ($\geq 20\%$) at the interface between the silica and water, our simulations show only a 5% density increase at the interface in both the 3 and 7 nm simulations. Previous simulations using rigid water and rigid silica, manually hydroxylated, showed ~20% increase in water density at the interface with amorphous silica in cylinders[9,11,42] or with nonrigid silica in a film with nonreactive water.[41] Interfacial water density increasing ~50% over bulk water was observed in simulations of water films confined in crystalline silica using rigid silica and water.[42,43] The dissociative potential allows water molecules to react with the silica surface, forming silanols at a concentration of 5.5 SiOH/nm^2, similar to the values from 3 to 6 SiOH/nm^2 observed experimentally.[44] This value is slightly higher than the ~4.0 SiOH/nm^2 (which includes the SiOH and $2 \times$ SiOH$_2$) observed in our previous simulations of the silica surface exposed to water vapor.[14] These dissociatively chemisorbed water molecules are shown in the figure as the distribution of oxygen from the water that attached to a silicon (labeled Ow-Si) and hydrogen attached to any oxygen that is attached to a silicon (H on silanols and labeled H-OSi).
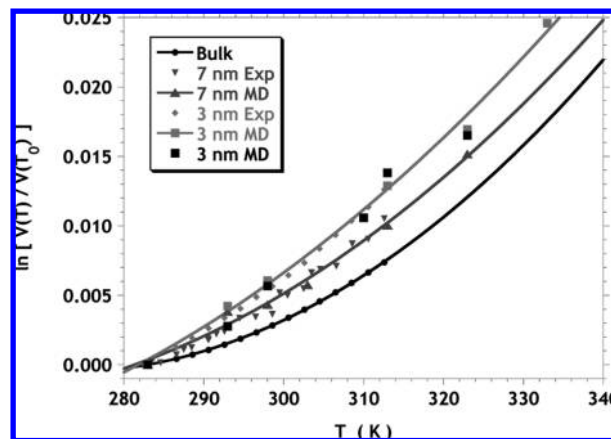

Figure 7. Comparison between MD simulations of the normalized volume change of the confined water and the experimental data for 30 and 70 Å pores. Also shown are the data for bulk water (which are the same for the experiment and simulation). The curves are parabolic fits.
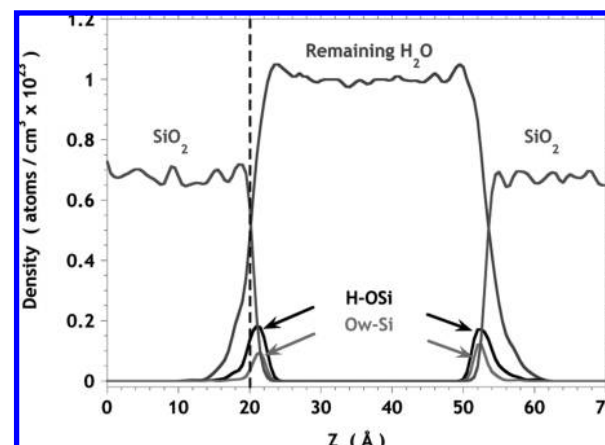

Figure 8. Density profiles of species as a function of distance perpendicular to the water/silica interfaces at 298 K and 1 atm. Remaining H$_2$O = water molecules remaining after reactions with glass, Ow-Si = oxygen originally in water that chemisorbed and bonded to Si, and H-OSi = hydrogen attached to any O that is bonded to Si. The latter two species indicate silanols. Vertical dashed line at 20 Å is the starting position for further analysis of structure.

The reactions and penetration of water extend about 7 Å below the outermost surface oxygen.

The effect of confinement is most clearly seen by evaluating the structure of the water over 3 Å thick slices parallel to the water/silica interface, starting at the 20 Å location shown by the vertical line in Figure 8. The oxygen−oxygen pair distribution functions (OO PDFs) are shown in Figure 9, along with the result for bulk water (similarly calculated and summed over 3 Å thick volumes), as shown previously.[40] Clearly, the interior of the 3 nm film has an OO PDF similar to bulk water, while water closer to the interface ($0-3$ Å, $3-6$ Å) shows a distinctly different structure. The water in the $0-3$ Å slice is quite different from bulk water but exists in the atomically rough silica surface and is templated by this surface. Experimental data for confined water similarly show alteration in the OO PDF.[45] The increase in the intensity in the first minimum near the interface is similar to the behavior seen

(40) Garofalini, S. H.; Mahadevan, T. S.; Xu, S.; Scherer, G. W. *ChemPhysChem* **2008**, *9*, 1997−2001.
(41) Hassanali, A. A.; Singer, S. J. *J. Phys. Chem. B* **2007**, *111*, 11181−11193.
(42) Giovambattista, N.; Rossky, P. J.; Debenedetti, P. G. *Phys. Rev. E* **2006**, *73*, 041604.
(43) Lee, S. H.; Rossky, P. J. *J. Chem. Phys.* **1994**, *100*, 3334−3345.
(44) Zhuravlev, L. T. *Langmuir* **1987**, *3*, 316–318.

(45) Ricci, M. A.; Bruni, F.; Gallo, P.; Rovere, M.; Soper, A. K. *J. Phys.: Condens. Matter* **2000**, *12*, A345–A350.
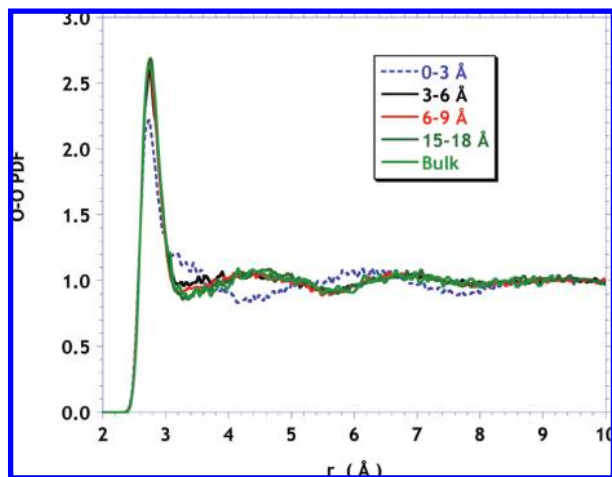
Figure 9. Oxygen−oxygen pair distribution functions (OO PDFs) of nanoconfined water as a function of distance from the water/silica interface showing that the structure of the water is altered by the interaction with the silica surface, decreasing as a function of distance from the interface. The effect extends nearly 1 nm, after which the interior of the film (15−18 Å in this figure) is exactly the same as bulk water.

in bulk water at higher temperature or higher pressure. Figure 10 compares the OO PDF of bulk water at $T = 298$ and 373 K, showing the increase in the intensity at the first minimum and a shift in the second OO peak, similar to the shifts observed in Figure 9 for the water closer to the interface (3−6 Å). However, the intensity of the first maximum decreases at elevated temperature in comparison to that of the confined water. The average density seen in the 3−6 Å slice in Figure 8 is similar to the density of bulk water at a pressure near 75 MPa. The OO PDF of the 3−6 Å slice is quite similar to that of bulk water at 75 MPa, as shown in Figure 11. Also shown in the figure are data for the OO PDF at higher T at $P = 0.1$ MPa and higher T and P. Higher T always causes a decrease in the first maximum intensity, although higher pressure compensates for this slightly. Higher T alone does not reproduce the structure in the 3−6 Å slice of the confined water. The influence of the atomically rough silica surface on the structure of the water adsorbed into that surface (0−3 Å) prevents a similar comparison to that slice.

6. Discussion

The molecular dynamics simulations indicate that there is a layer about 0.6 nm thick adjacent to the surface of the pore wall in which the structure is quite different from that of bulk water. That layer has certain features in common with bulk water at elevated temperature and pressure; this is consistent with our experiments, since raising either T or P increases the volumetric coefficient of thermal expansion (CTE) of water. The MD simulations have been shown to indicate that the average CTE of the 0.6 nm layer is about $5.9 \times 10^{-4}\,°C^{-1}$ and varies little with temperature over the range examined (10−40 °C).[40] In this section, we will show that the trend in CTE with pore size shown in Figure 3 can be explained on the basis of the volume fraction of the pore volume occupied by the 0.6 nm layer of anomalous water.

For a cylindrical pore with radius r_p containing a surface-affected layer with thickness δ, the volume fraction of the pore space occupied by that layer is

$$v = \frac{\pi r_p^2 - \pi(r_p - \delta)^2}{\pi r_p^2} = \frac{2\delta}{r_p} - \frac{\delta^2}{r_p^2} = s\delta\left(1 - \frac{s\delta}{4}\right) \quad (3)$$
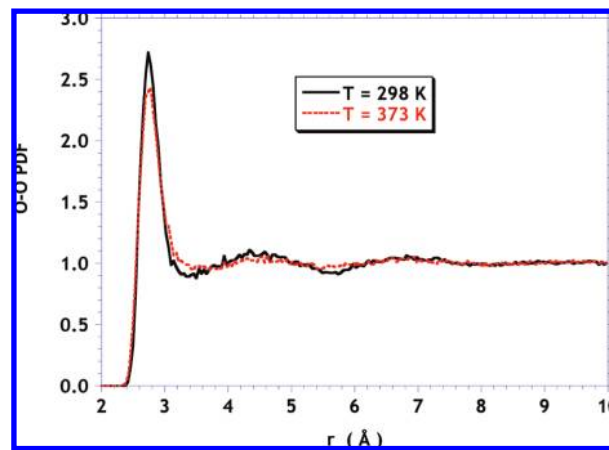

Figure 10. OO PDF for bulk water at 1 atm and 298 and 373 K, showing the change in the structure with temperature. The change is similar to that near the interface of the confined film.
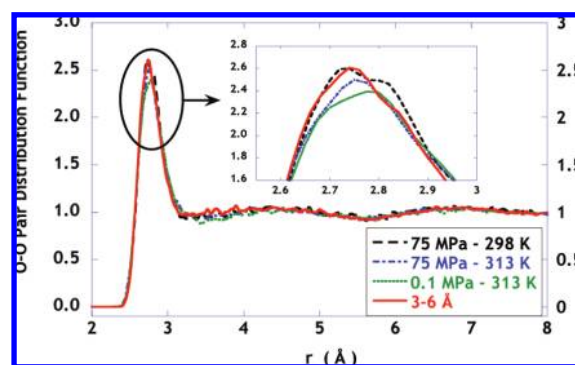

Figure 11. Oxygen−oxygen pair distribution function for water in layer 3−6 Å from glass surface (at $T = 298$ K and $P = 0.1$ MPa) compared to pdf for bulk water at different P and T. Bulk water at higher P (298 K, 75 MPa) has a structure closer to that of confined water than bulk water at higher T alone (313 K, 0.1 MPa) or higher T and P (313 K, 75 MPa).

The second equality uses the definition $r_p = 2/s$, where $s = S/V_p$, $S = $ BET surface area, and $V_p = $ specific pore volume. The values of these quantities are given in Table 1. We can estimate the average thermal expansion of the pore liquid, α, in terms of that of the bulk liquid, α_B, by volume averaging:

$$\alpha = v\alpha_S + (1-v)\alpha_B \quad (4)$$

where α_S is the thermal expansion coefficient of the anomalous (surface-affected) layer. The volume of the pore water, which was measured in the experiments, is given by

$$\ln\left(\frac{V(T)}{V(T_0)}\right) = \ln(1 + \int_{T_0}^{T} \alpha(y)\, dy) \quad (5)$$

In the following calculations, we treat α_S as a constant but use the known temperature dependence for α_B. On the basis of data from ref 46, we obtain the following approximation for the range $-10 \leq T\,(°C) \leq 70$:

$$\alpha_B \doteq -5.379 \times 10^{-5} + 1.530 \times 10^{-5}T - 1.341 \times 10^{-7}T^2 +$$
$$6.480 \times 10^{-10}T^3 + 1.960 \times 10^{-24}T^4 - 5.310 \times 10^{-26}T^5$$
$$(6)$$

(46) Dean, J. A., Ed. *Lange's Handbook of Chemistry*; McGraw-Hill: New York, **1973**.

Equations 3−6 were used to fit the experimental data, allowing α_S and/or δ to be adjustable. In addition to the data shown in Figure 3, one experiment was done in which the Vycor sample with 7 nm pores was cooled to −10 °C. Those data were fit separately, as discussed below.

When both parameters are adjustable, the fitted curves all pass through the data, well within the experimental uncertainty. However, as shown in Table 2, the parameters are rather erratic. Since the MD simulations indicate that the thickness of the surface-affected layer is the same in gaps of 3 and 7 nm, we impose an equal value of δ on all the samples and adjust only the CTE of the layer. The results, shown in Table 3, are quite consistent. The thinner that δ is assumed to be, the larger the expansion in that layer has to be to account for the measured expansion. When the assumed thickness is close to that found from MD ($\sim 6\,\text{Å}$), then the expansion of the layer is found to be $5 \times 10^{-4}\,°C^{-1}$, which is quite similar to the value of $5.9 \times 10^{-4}\,°C^{-1}$ that was obtained from the simulations.[40]

The quality of the fits is shown in Figure 12. For the samples with pore diameters of 13, 7, and 5 nm, the fits are excellent for $10 \leq T\,(°C) \leq 40$, and the quality of the fit is the same when δ is assumed to be 0.5 or 0.6 nm. There is a slight discrepancy for the data obtained at lower temperature (Figure 12b), presumably because the structure or thickness of the layer changes at low T, but the measurements and calculations both indicate that the density maximum is broadened and pushed down to at least −8 °C. No MD simulations were done in that range. The poorest agreement is for the xerogel with 3 nm pores, as shown in Figure 12d. The discrepancy is not large, but it is systematic and might be related to the microporous tail of the pore size distribution indicated in Figure 2a. On the whole, it is fair to say that the measured expansion of the confined water is accurately predicted by a simple volume average of the properties of the surface-affected layer and bulk water.

Table 2. Fit with Two Free Parameters: δ and α_S

sample ID	δ (nm)	$10^4 \times \alpha_S$ $(°C^{-1})$
Vycor 5 nm	0.32	7.8
Vycor 7 nm	0.36	7.4
Vycor 7 nm (low)[a]	0.021	85.0
Xerogel 3 nm	0.60	4.4
Aerogel 13 nm	0.086	22.0

[a] Fit including data for $-10 \leq T\,(°C) \leq 10$.

Table 3. Values of $10^4 \times \alpha_S$ $(°C^{-1})$ from Fits with δ (nm) Fixed

sample ID	$\delta = 0.30$	$\delta = 0.50$	$\delta = 0.55$	$\delta = 0.60$	$\delta = 0.65$
Vycor 5 nm	8.1	5.9	5.6	5.3	5.1
Vycor 7 nm	8.4	6.0	5.7	5.4	5.2
Vycor 7 nm (low)[a]	7.5	5.1	4.8	4.5	4.3
Xerogel 3 nm	6.1	4.7	4.6	4.4	4.3
Aerogel 13 nm	7.8	5.5	5.2	5.0	4.7
average[b]	7.6	5.5	5.2	5.0	4.8

[a] Fit including data for $-10 \leq T\,(°C) \leq 10$. [b] Average of values for Vycor5, Vycor7 (not including low T), Xerogel, and Aerogel.
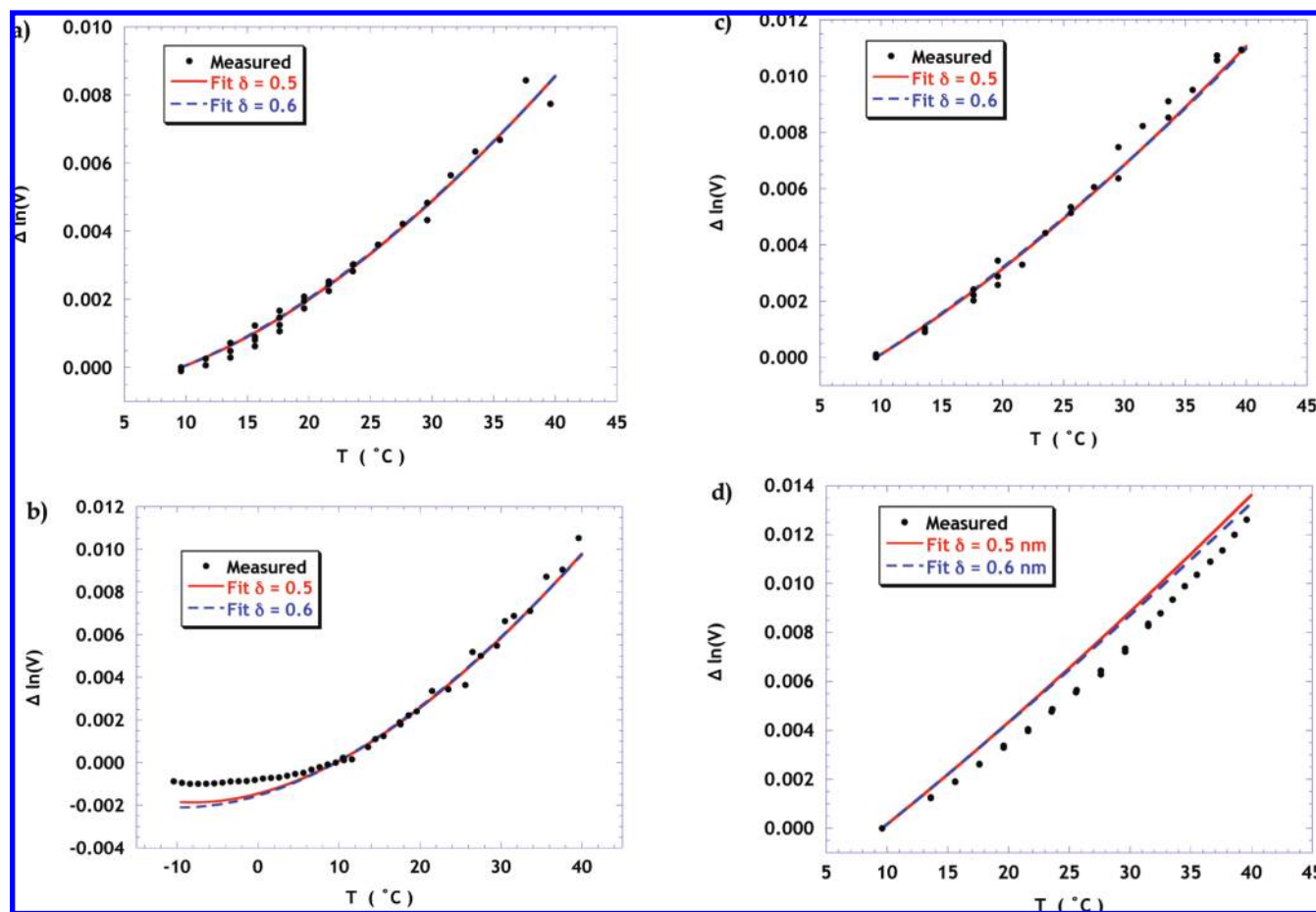

Figure 12. One-parameter fits to the thermal expansion data for (a) Aerogel 13 nm, (b) Vycor 7 nm, (c) Vycor 5 nm, and (d) Xerogel 3 nm, where $\Delta\ln(V) = \ln V(T) - \ln V(9.6\,°C)$. Fit parameters are given in Table 3.

One of the important results obtained by using the dissociative water potential is that we are able to accurately simulate the interactions and reactions between water molecules and the silica surface. This has shown to be vitally important in these simulations as they show that water molecules can break strained siloxane bonds (Si−O−Si) in the surface of the glass, opening the surface to further penetration by water molecules. Density profiles show the presence of silanol sites together with H_2O molecules in the subsurface (∼1 nm below the outermost oxide surface). These constrained water molecules may play an important role in the experimental NMR observation that diffusion of water at the interface is an order of magnitude slower than bulk water.[47,48] Measurements on Vycor glass have shown that the permeability decreases as the molecular size of the liquid increases.[49,50] The data can be explained quantitatively by assuming that there is a monolayer of molecules that are immobilized on the pore wall.[47] In the case of water, the agreement is better if it is assumed that two molecular layers (about 0.6 nm) are immobilized. In another paper, we will compare the transport behavior of confined water found from measurements of permeability and diffusivity with the predictions of the MD simulations. As with the CTE, we will see that the mobility of water is not much affected by 1 M NaCl but is affected by $CaCl_2$.

(47) Almagor, E.; Belfort, G. *J. Colloid Interface Sci.* **1978**, *66*, 146−152.
(48) Halperin, W. P.; Bhattacharija, S.; D'Orazio, F. *Magn. Reson. Imaging* **1991**, *9*, 733−737.
(49) Debye, P.; Cleland, R. L. *J. Appl. Phys.* **1959**, *30*, 843−849.
(50) Vichit-Vadakan, W.; Scherer, G. W. *J. Am. Ceram. Soc.* **2000**, *83*, 2240−2245. Erratum: *J. Am. Ceram. Soc.* **2004**, *87*, 1614.